FISEVIER

Contents lists available at ScienceDirect

# Journal of Colloid And Interface Science

journal homepage: www.elsevier.com/locate/jcis



# Regular Article

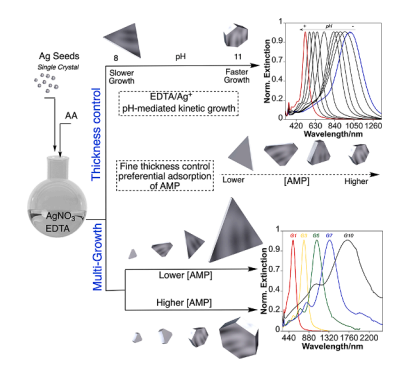


# Precise control of silver nanoplate dimensions and optical properties via pH, EDTA and AMP mediated synthesis

Adrián Fernández-Lodeiro <sup>a,b,1</sup>, Carlos Fernández-Lodeiro <sup>c,d</sup>, Silvia Nuti <sup>a,b</sup>, Ignacio Pérez-Juste <sup>c,d</sup>, Isabel Pastoriza-Santos <sup>c,d</sup>, Jorge Pérez-Juste <sup>c,d,\*</sup>, Enrique Carbo-Argibay <sup>e</sup>, José Luis Capelo-Martínez <sup>a,b</sup>, Carlos Lodeiro <sup>a,b</sup>, Javier Fernández-Lodeiro <sup>a,b,\*\*</sup>

- <sup>a</sup> BIOSCOPE Research Group, LAQV-REQUIMTE, Chemistry Department, NOVA School of Science and Technology, FCT NOVA, Universidade NOVA de Lisboa, 2829-516 Caparica, Portugal
- <sup>b</sup> PROTEOMASS Scientific Society, Costa de Caparica, 2825-466, Portugal
- <sup>c</sup> CINBIO, Universidade de Vigo, Campus Universitario As Lagoas, Marcosende, 36310 Vigo, Spain
- <sup>d</sup> Departamento de Química Física, Universidade de Vigo, Campus Universitario As Lagoas, Marcosende, 36310 Vigo, Spain
- <sup>e</sup> International Iberian Nanotechnology Laboratory INL, Avenida Mestre José Veiga s/n, 4715-330 Braga, Portugal

#### GRAPHICAL ABSTRACT



# ARTICLE INFO

# Keywords: Silver nanoplates Seed-mediated Thickness control Tunable optical response Ethylenediaminetetraacetic (EDTA) Adenosine 5'-monophosphate (AMP)

#### ABSTRACT

We present a seed-mediated synthesis method for producing silver nanoplates (AgNPTs) with customizable size and thickness, ensuring high yield and precise optical properties. This approach leverages ethylenediamineterracetic acid (EDTA) as a key component in the synthesis process, utilizing small single-crystal silver seeds. The interaction between  $Ag^+$  ions and EDTA at varying pH levels dynamically regulates silver complexation and reduction kinetics during seed overgrowth, leading to the formation of truncated nanoplates with superior optical responses. By adjusting the pH within the range of 8–10.5, we can manipulate the growth of

 $\textit{E-mail addresses:} \ juste@uvigo.gal\ (J.\ P\'erez-Juste),\ j.lodeiro@fct.unl.pt\ (J.\ Fern\'andez-Lodeiro).$ 

#### https://doi.org/10.1016/j.jcis.2024.10.179

<sup>\*</sup> Corresponding author at: CINBIO, Universidade de Vigo, Campus Universitario As Lagoas, Marcosende, 36310 Vigo, Spain.

<sup>\*\*</sup> Corresponding author at: BIOSCOPE Research Group, LAQV-REQUIMTE, Chemistry Department, NOVA School of Science and Technology, FCT NOVA, Universidade NOVA de Lisboa, 2829-516 Caparica, Portugal.

<sup>&</sup>lt;sup>1</sup> Present Addresses: Department of Electrical and Computer Engineering, University of Cyprus, Nicosia 2109, Cyprus.

the nanoplates, enabling a flexible optical response ranging from 519 to 1006 nm due to changes in their size and thickness. Additionally, nanoplate overgrowth extends plasmon resonance up to approximately 2000 nm. The incorporation of Adenosine 5' monophosphate (AMP) not only enhances nanoplate stability but also allows for precise thickness adjustment independent of growth kinetics. This method provides a systematic approach to tailor nanoplate morphology and optical properties with unprecedented precision. The role of EDTA is attributed to its complexation ability with  $Ag^+$  and its assistance in facet evolution, supported by density functional theory (DFT) simulations of surface energies modified by EDTA adsorption. Furthermore, DFT calculations confirm that AMP can further modify the surface energies of different facets, enabling precise thickness control.

#### 1. Introduction

Nanoplates (NPTs) showcase one of the most intriguing nanoscale geometries among noble metal nanoparticles. Their two-dimensional structure, varying from triangular to hexagonal shapes, induces a high degree of anisotropy, resulting in a highly tunable optical response. Among these, silver nanoplates (AgNPTs) are particularly noteworthy due to their high extinction coefficient, tunable Localized Surface Plasmon Resonance (LSPR), and exposed crystal facets with high surface energy, making them particularly promising for various optical and catalytic applications [1–3].

Mirkin and colleagues pioneered the production of AgNPTs through plasmon-mediated synthesis. AgNPTs are formed through photochemical reduction, leveraging plasmon excitation to control the growth. Light-induced oscillation of electrons enhances the reduction of silver ions, promoting the controlled growth of well-defined NPTs [4,5]. Subsequently, over the last two decades, significant efforts have been devoted to unravelling the growth mechanism and developing new methodologies to produce this fascinating nanoscale geometry, aiming to control and leverage its unique optoelectronic properties.

In addition to light-mediated synthesis, which has achieved high morphological control [5,6], other strategies, both seed-mediated or seedless, have been developed to obtain AgNPTs with controlled lateral length and tunable optical response. Thus, different capping ligands have been employed such as polyvinylpyrrolidone (PVP) [7–11], cetyltrimethylammonium bromide (CTAB) [12,13], Pluronic F127 [14], tannic acid [15], glycyl glycine [16], polystyrene sulphonate (PSS) [17,18], ethylenediaminetetraacetic sodium salt (EDTA) [19], among others [20–22]. Table S1 in the Supporting Information summarizes the most significant synthesis protocols reported to date, with special emphasis on the growth strategy, the shape-inducing agent or stabilizer, the side length, and the thickness control, as well as LSPR tunability and nanoplate yield.

The preferential adsorption of molecular entities on specific crystallographic faces has been recognized as a key factor in the synthesis of AgNPTs, promoting face-selective growth. However, the discovery of forbidden 1/3(4 2 2) reflections in their 2D crystalline structure, caused by stacking faults parallel to {1 1 1} faces, has highlighted the importance of these defects in the development of Ag nanoplate structures [23]. Recently, the stacking fault structure of AgNPTs was resolved, revealing various types of surfaces on their lateral sides, such as concave, step, and  $\{1\ 0\ 0\}$  faces. These regions provide sites for adding atoms with a higher coordination number compared to the flat {1 1 1} faces on the top and bottom, leading to anisotropic growth along the 2D direction and supporting the theory of stacking fault-induced 2D growth [24]. However, the origin of stacking defects remains elusive. Some studies suggest that these defects in the crystalline structures of the seed may be fundamental in the subsequent development of 2D structures of AgNPTs, though the evidence is limited due to the scarcity of research analyzing the crystal structure of the seeds (see Table S1) [21,25,26].

Furthermore, it is noteworthy that many synthetic processes tend to converge towards slow growth regimes, which favor the addition of atoms within entrance grooves formed in stacking fault regions. Consequently, crystal growth predominantly occurs along the  $[1\ 1\ 1]$  direction and parallel to the plane  $\{1\ 1\ 1\}$  [10,19,26-28]. In this context,

molecules such as sodium citrate (SC) play a critical role in the seed-mediated synthesis of NPTs. Beyond preferential adsorption, sodium citrate acts as a silver complexing agent, modulating ionic diffusion and growth kinetics, thus providing more controlled conditions for AgNPTs growth [10,26]. Other molecules, including polyacrylamide [27], acetonitrile [29,30], or EDTA [19] among others, have also been identified as chelating agents that manipulate the kinetic reduction.

The optical properties of AgNPTs are primarily determined by their geometry, especially their lateral size, thickness and degree of truncation. Thus, an increase in the lateral size or a decrease in the degree of truncation typically leads to a red-shift in the main LSPR, as this implies an increase in the aspect ratio (ratio of lateral dimension to thickness) [10,12,30,31]. Different reports have shown that AgNPTs can achieve tunable LSPRs of up to 3000 nm by modulating their lateral dimensions to the order of microns [10,30]. Interestingly, while lateral size tunability of AgNPTs has been extensively studied, controlling thickness has proven more challenging. Note that thickness variation significantly alters the aspect ratio, providing greater control over the optical response. Metraux and Mirkin achieved some control over AgNPTs thickness using a seedless synthesis with PVP, SC and hydrogen peroxide [7]. Since then, similar strategies have shown thickness tuning in the 5–10 nm range [32,33].

Using a seed-mediated strategy, Charles and coworkers were able to modulate the thickness from approximately 5 nm to 14 nm by varying the amount of seed, although the optical response of the AgNPTs did not extend beyond 1200 nm [18,31]. Additionally, Zeng and collaborators demonstrated that SC and PVP concentrations affect vertical versus lateral growth during successive epitaxial deposition on AgNPTs [34], although the optical response was not documented (see Table S1). Finally, combining PVP with *N*-methylpyrrolidone has produced AgNPTs with thicknesses ranging from 8 to 63 nm. Nevertheless, this increase in thickness was accompanied by a large increase in size, resulting in a low aspect ratio and LSPR responses below 1000 nm [35], This seedless approach, while producing nanoplates, led to broad LSPR bands, compromising monodispersity. Thus, despite significant progress in manipulating the morphology of AgNPTs, achieving precise control over their thickness remains challenging.

Building on these insights and taking into consideration that EDTA exhibits strong chelating ability to silver cations, which may alter their reduction potential, activation energy, and ionic diffusion coefficient [36,37], we aim to develop a seed-mediated approach using EDTA to produce uniform AgNPTs with high yield and precise control over their lateral dimensions and thickness. This method aims to achieve tailored optical responses in the visible to near-infrared (NIR) region. By controlling the pH within a specific range or adding 5'-adenosine monophosphate (AMP), we can modulate the thickness of AgNPTs. The ability of this strategy to vary both the thickness and lateral dimensions of AgNPTs allows for precise tailoring of their optical response, opening new opportunities in nanoplasmonics. Our results demonstrate the preferential formation of Ag {1 1 1} facets stabilized by EDTA molecules, as predicted by density functional theory (DFT) surface energy calculations. Additionally, DFT simulations support that the preferential adsorption of AMP on {1 0 0} or {1 1 0} crystal facets drives the thickness control of AgNPTs.

#### 2. Results and discussion

Our central hypothesis originated from the commonly accepted statement that the crystal structure of the seeds defines the crystallinity of the final nanoparticles [38]. Thus, we propose that leveraging EDTA's potent chelating capabilities with Ag<sup>+</sup> in the presence of well-defined tiny silver seeds could present an intriguing method for producing monodisperse AgNPTs in high-yield. To test this, we firstly optimized the production of tiny single-crystal Ag seeds via chemical reduction using NaBH4, with EDTA acting as stabilizer. The protocol involved adding Ag(I):EDTA (1:2 molar ratio) solution into a NaBH4 solution at a constant rate of 1 mL/min (see materials and methods). The resulting Ag seeds exhibited a LSPR centered at 395 nm and a mean size of approximately 4.8  $\pm$  1.6 nm (Fig. 1). High-resolution transmission electron microscopy (HRTEM) analysis confirmed a high population of single crystal face-centered cubic (fcc) AgNPs with an interplanar distance of 0.235 nm that belongs to Ag (1 1 1), as confirmed by Fast Fourier Transform (FFT) (Fig. 1B). A minor presence of twinned or multitwinned seeds was also observed (Fig. S1).

These seeds were grown via autocatalytic reduction in the presence of silver ions, EDTA and ascorbic acid (AA). The optimized experimental conditions reveal that a Ag(I):EDTA ratio of 1:4, which produces a pH of ca. 9.3, gives rise to truncated AgNPTs with yield >90 % and with an LSPR band centered at ca. 830 nm (see Fig. S2). It is important to note that seeds prepared under different experimental conditions led to Ag NPs constituted by mixtures of nanospheres and plates (data not shown). We further explored the tunability of the main LSPR by varying the amount of seed added to the growth solution while keeping an Ag(I): EDTA ratio of 1:4. As shown in Fig. 2A, increasing the seed volume from 0.15 mL to 5 mL results in a blue-shift in the main LSPR band from 830 nm to 519 nm. This observed shift in the LSPR can be ascribed to a decrease in the overall aspect ratio (AR) of the silver plates.

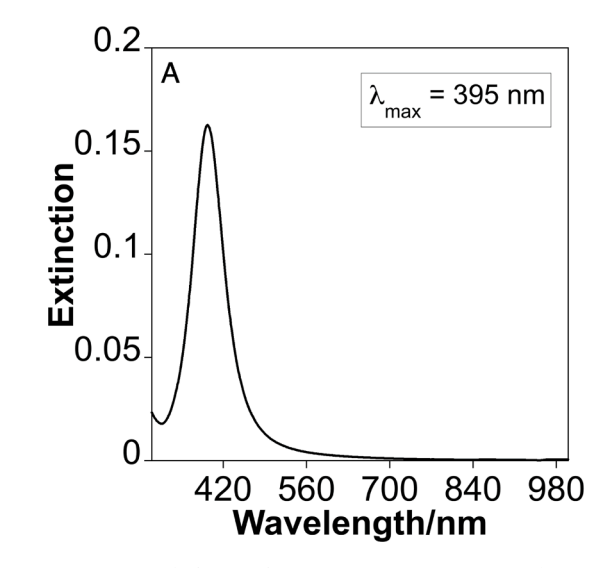
Given that EDTA's ability to chelate silver cations is pH-dependent, we investigated its effect on the growth of nanoplates across a pH range from 7 to 12, while keeping the concentrations of silver nitrate, ascorbic acid and EDTA, and the volume of seed constant. As shown in Fig. 2B, increasing the pH from 8.1 to 10.5 resulted in a blue-shift of the main LSPR band from approximately 1006 nm to 519 nm, with a linear relationship between pH and LSPR band position (see Fig. 2C). Additionally, the plasmon band became narrower as the pH increased. TEM analysis confirmed the formation of truncated AgNPTs in all samples, with higher pH values leading to greater truncation, shorter side lengths of the AgNPTs, and increased thickness. These morphological changes

reduced the AR, corresponding with the observed blue-shift in the LSPR band. For example, AgNPTs formed at pH 8.1 had a size and thickness of  $110.1 \pm 13.8$  nm and  $7.0 \pm 1.1$  nm, respectively (AR of 15.7). At pH 10.5, the NPTs measured  $59.5 \pm 4.3$  nm and  $17.1 \pm 1.0$  nm (AR of 3.5) (see Fig. 2D-G and S3). Below pH 8, the reaction slowly produced polydisperse AgNPTs, indicated by a very broad optical response (Fig. S4A). Conversely, above pH 11.5, the reaction proceeded more rapidly, resulting in the formation of pseudo-spherical nanoparticles (Figures S4B-D). Importantly, our protocol allows for modulation of the thickness of AgNPTs by simply adjusting the pH while using the same volume of seeds. Unlike previous methods, this approach does not require additional stabilizers [34,35], changes in seed quantity [18,31], or multiple growth steps [34].

To investigate the effect of the pH on the formation mechanism, we conducted a time-resolved spectrophotometric study of the NPT growth at different pHs. Fig. 3 presents the time-evolution UV–Vis-NIR spectra of AgNPTs growth at pH 9.9, 9.5 and 8.1. Initially, the in-plane LSPR band appears at lower wavelengths, and gradually increases in intensity and red-shifting over time. Notably, the traces of the time-dependent red-shift of the main LSPR band, as shown in Fig. 3D, indicate faster growth at a higher pH (9.9), with the LSPR band stabilizing after 15 min. As the pH decreases to 9.5 and 8.1, the growth kinetics slow significantly, with the LSPR band stabilizing after *ca.* 40 min and 70 min, respectively. This deceleration is accompanied by a gradual red-shift of the LSPR band from 650 nm to 1006 nm.

Given that an increase in the volume of seeds added at constant pH leads to a progressive blue-shift of the LSPR band, we explored the possibility of carrying out the growth in multiple steps by adding a fixed volume of the initial growth solution into a freshly prepared growth solution for each subsequent step (see experimental section for details). The extinction spectra of the resulting plates after each growth step, as shown in Fig. S5 of the Supplementary Information, demonstrate the potential to achieve plasmonic bands extending up to *ca.* 2000 nm.

Next, to fine-tune the thickness of the nanoplates and consequently their optical properties, we investigated promoting vertical over lateral growth by introducing additional stabilizers and capping ligands. Among the different ligands available, we selected AMP due to its ability to stabilize silver nanoparticles [39]. Moreover, AMP exhibits preferential adsorption on specific facets of noble metals at the nanometric scale [40], a characteristic that holds potential advantages in our current context. We investigated the effect of increasing AMP concentrations ([AMP]), ranging from 0.075 mM to 0.7 mM, on a standard AgNPTs synthesis at pH 8.1. In the absence of AMP, the AgNPTs exhibited a main



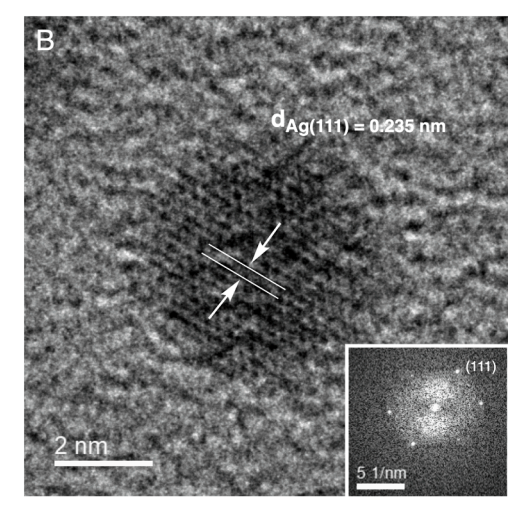


Fig. 1. (A) Extinction spectrum of silver seeds in water. (B) HRTEM image of one Ag seed showing its single crystal structure with an interplanar distance of 0.235 nm assigned to Ag(111). The inset shows the Fast Fourier Transform (FFT) obtained from B.

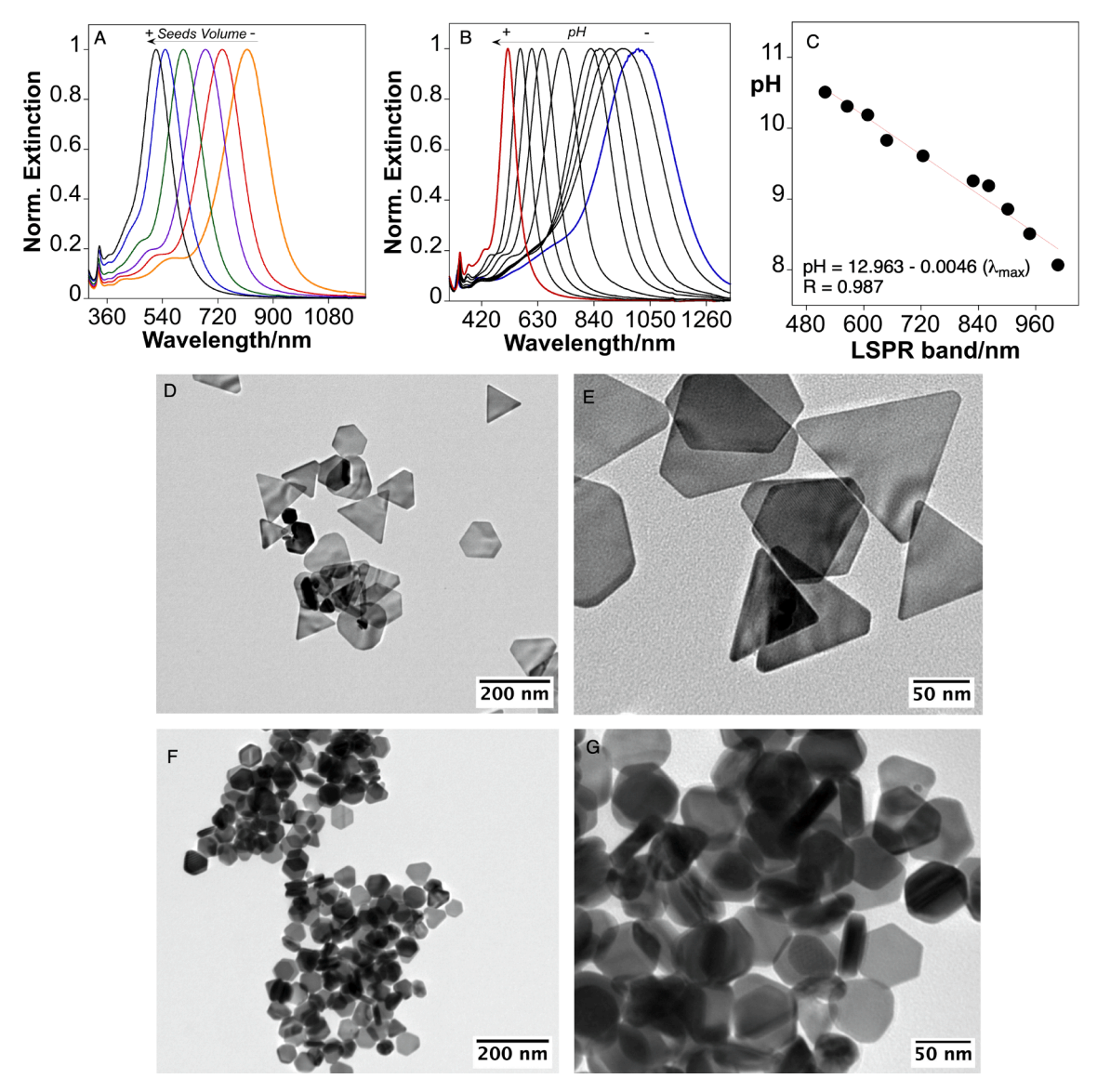


Fig. 2. (A) Extinction spectra of AgNPTs obtained using [AgNO $_3$ ], [EDTA], [AA] of 0.15 mM, 0.60 mM, 0.15 mM respectively and varying seed volume between 0.15 and 5 mL. (B) Extinction spectra of AgNPTs obtained at different pH values ranging from 8.1 (blue spectra) to 10.5 (red spectra). In all the synthesis, the volume of seeds was 0.15 mL. (C) Evolution of the  $\lambda_{max}$  of the main LSPR as a function of pH. (D-G) Representative TEM images of AgNPTs obtained at pH 8.1 (D,E) and pH 10.5 (F,G). (For interpretation of the references to colour in this figure legend, the reader is referred to the web version of this article.)

LSPR band centered at ca. 1006 nm (Fig. 2B, blue spectrum). The addition of AMP led to a gradual blue-shift of the main LSPR band, with negligible contributions from other morphologies. Specifically, increasing the [AMP] from 0.075 mM to 0.7 mM (corresponding to Ag (I):AMP molar ratios ranging from 1:0.5 to 1:4.6, see experimental section for details) resulted in AgNPTs with the main LSPR band shifting from 921 nm to 554 nm (see Fig. 4A). Characterization of the obtained particles by TEM confirms that the presence of AMP does not affect the AgNPTs yield but does reduce their lateral dimensions. For instance, increasing the [AMP] from 0.15 mM to 0.6 mM decreased the average edge length from 93.2  $\pm$  10.5 nm to 69.9  $\pm$  5.5 nm (see Fig. 4C,E). Concurrently, the nanoplate thickness increased from 9.1  $\pm$  0.8 nm to 15.1  $\pm$  0.7 nm (see Fig. 4D,F), leading to an overall decrease in the aspect ratio from 10.2 to 4.6, which accounts for the observed plasmon tunability (see Fig. 4B and Fig. S6). It should be noted that the increase in [AMP] is accompanied by an increased degree of truncation of the plates (see Fig. S7A-F). Notably, nanoplates synthesized with AMP exhibited enhanced stability and resistance to oxidation, enabling their purification and long-term storage with minimal changes in their optical

response (Fig. S7G, H).

Interestingly, AMP did not affect the growth kinetics, with the growth process taking approximately 90 min regardless of [AMP] (Figs. 3 and S8). Furthermore, the presence of AMP did not significantly change the pH of the medium, which varied from 8.1 in the absence of AMP to 8.6 at 0.7 mM AMP. Therefore, it can be concluded that while the solution pH governs the growth kinetics, AMP modulates the thickness and, thus, the AR of the AgNPTs, suggesting a strong interaction between AMP and silver surfaces during nanoplate growth. Next, we explored the effect of the seeds volume in the presence of 0.15 mM AMP. As expected, varying the seed volume from 0.15 mL to 5 mL led to AgNPTs with tunable LSPR bands ranging from 867 nm to 503 nm, respectively. However, when the [AMP] was increased to 0.6 mM, the position of the LSPR band could only be tuned from 619 nm to 474 nm within the same volume range. This indicates that higher seed volumes can be used to produce smaller AgNPTs with adjustable thickness (see Figs. S9 and S10).

To assess whether the thickness of the AgNPTs can be manipulated through successive growth steps by varying the [AMP], we investigated

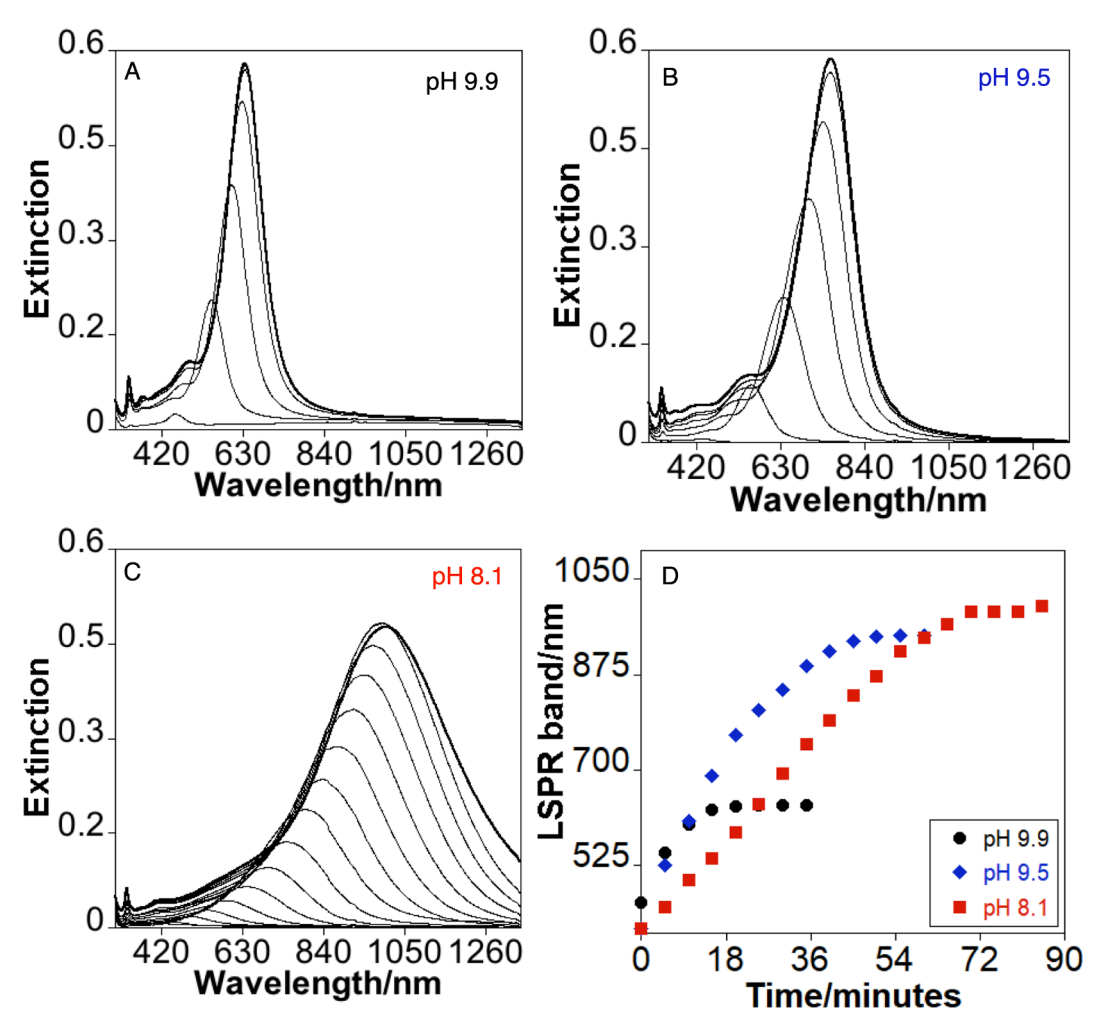


Fig. 3. (A-C) Time-resolved UV–Vis-NIR spectra showing the growth of AgNPTs at different pHs: 9.9 (A), 9.5 (B), and 8.1 (C). (D) Time traces of the  $\lambda_{max}$  of the LSPR band for each pH.

their overgrowth to further tune their optical properties. This was done by conducting a multi-step growth process at two [AMP]. Fig. 5 shows the extinction spectra of AgNPTs obtained after various growth steps with [AMP] of 0.15 mM and 0.6 mM. In both cases, a gradual red-shift in the main LSPR band was observed during the multistep growth. After 10 growth steps AgNPTs with LSPR band at ca. 1717 nm and 1068 nm were obtained for [AMP] of 0.15 mM and 0.6 mM, respectively (Fig. 5A,D). The influence of [AMP] on the final optical properties is primarily attributed to changes in nanoplate thickness and the degree of truncation. At higher [AMP], the nanoplates become smaller, thicker and more truncated, resulting in a reduced aspect ratio (see Fig. 5B,C and E, F and Figs. S11 to S13). It should be noted that overgrowing nanoplates with optical response beyond 2000 nm resulted in a degree of coalescence and precipitation, with some nanoplates depositing on the magnetic stirrer and the walls of the reaction vessel. This indicates that the colloidal stability, governed by the electrostatic repulsion provided by EDTA and AMP, becomes insufficient to stabilize larger structures.

Before proposing a putative mechanism, the crystalline structure of AgNPTs was studied by HRTEM. A representative HRTEM image of a nanoplate corner is shown in Fig. 6A. The corresponding FFT reveals six bright spots with hexagonal symmetry, which can be indexed to the  $\{2\ 2\ 0\}$  reflections of the fcc crystal oriented along the  $[1\ 1\ 1]$  direction (Fig. 6B). This indicates that the flat surface of the particle is parallel to the  $\{1\ 1\ 1\}$  plane. Additionally, forbidden reflections at  $1/3\{4\ 2\ 2\}$  were observed in the FFT images, suggesting the presence of internal stacking faults in the nanoplate [23]. Atomic resolution TEM images further

corroborate these findings, displaying interplanar distances of 2.5 Å and 1.4 Å, corresponding to the  $1/3\{4\ 2\ 2\}$  forbidden reflections and the  $\{2\ 2\ 0\}$  Bragg reflections, respectively (Fig. 6C,D). When the nanoplates were vertically aligned with the electron beam, the presence of stacking faults running parallel along the  $\{1\ 1\ 1\}$  plane was confirmed, consistent with previous scientific reports [1,2] (Fig. 6E,F). Similar observations were obtained for thicker nanoplates (Fig. S14). However, in our study, the Ag seeds used to grow high-purity nanoplates mostly exhibit a single-crystal fcc structure (Fig. 1 and Fig. S2). This leads us to hypothesize that symmetry breaking in the single-crystalline seeds must occur during the early growth stages of the nanoparticles. Indeed, controlled growth of Ag seeds from approximately 4–19 nm revealed the formation of nanoparticles with nanoplate morphology (Fig. S9B), indicating that symmetry breaking of single-crystalline seeds within this size range.

Based on these observations we propose a growth mechanism based on the following key points:

– *EDTA complexation with silver ions.* EDTA plays a crucial role in the synthesis of AgNPTs by complexing with silver ions. The dissociation constants (pKa) of EDTA are as follows: for the carboxylic acid groups, pKa1 to pKa4 are 0.1, 1.5, 2.2, and 3.2, respectively. For the amino groups, pKa5 and pKa6 are 6.8 and 10.3, respectively, with slight variations depending on the ionic strength of the medium [41]. Within our specified pH range, all carboxyl groups are expected to be deprotonated [42]. However, the protonation states of the tertiary amino groups vary across a pH range from 8.1 to 10.5. This variability appears to be crucial

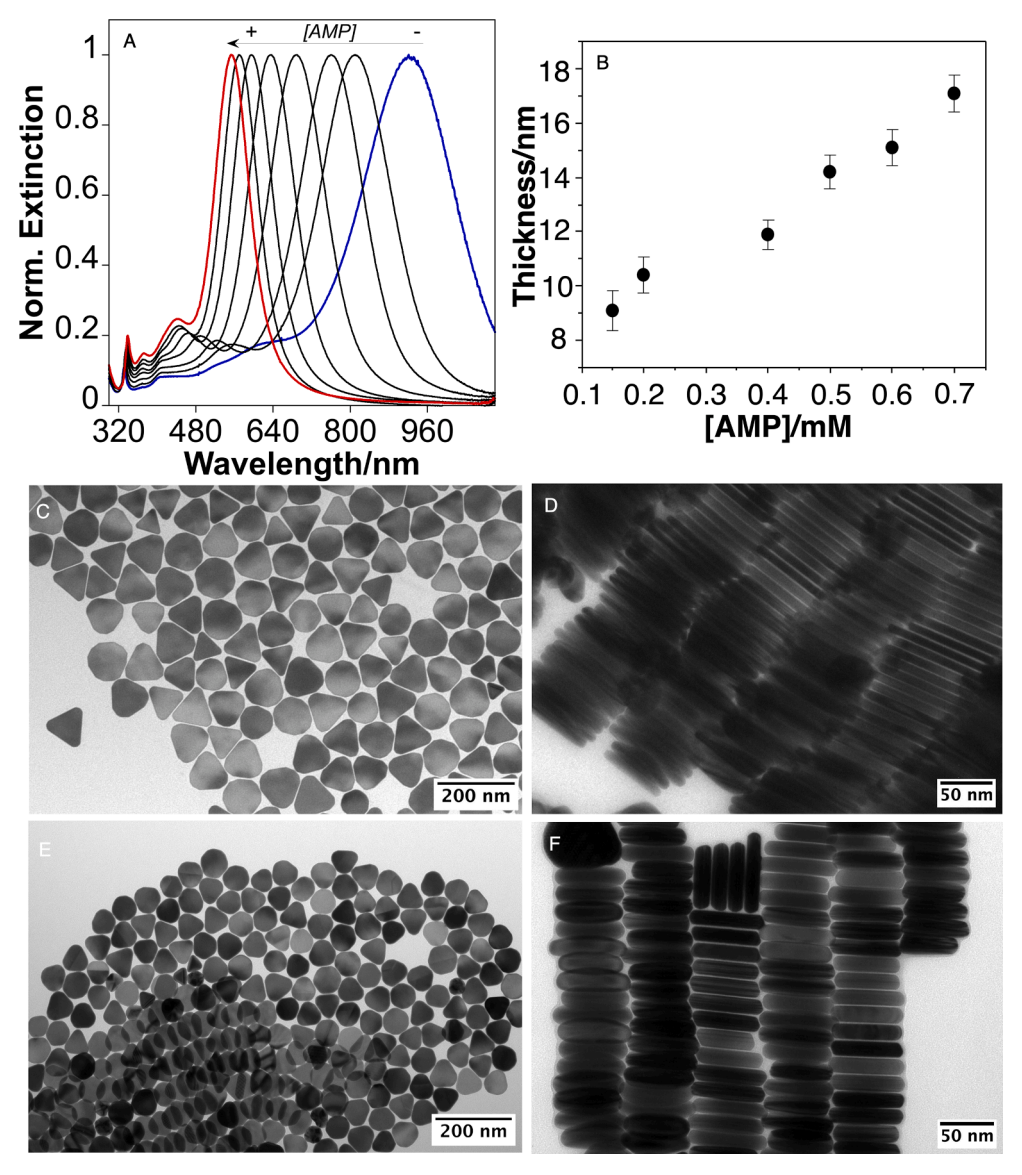


**Fig. 4.** (A) Extinction spectra of Ag nanoplates obtained in the presence of different [AMP] ranging from 0.075 mM (blue spectrum) to 0.7 mM (red spectrum). The concentration of AgNO<sub>3</sub>, EDTA, AA, H<sub>3</sub>PO<sub>4</sub> was 0.15 mM, 0.60 mM, 0.15 mM and 0.085, respectively, and the Ag seed volume was 0.15 mL in all cases. (B) Graphical representation of the thickness of the resulting AgNPTs as a function of [AMP]. (C-E) Representative TEM images of AgNPts obtained in the presence of 0.15 (C) and 0.6 (E) mM of AMP. (D,F) TEM images of stacking nanoplates obtained with 0.15 (D) and 0.6 (F) mM of AMP, revealing different thickness. (For interpretation of the references to colour in this figure legend, the reader is referred to the web version of this article.)

in the complexation and reduction of Ag(I) ions, influencing the kinetics of nanoplate growth.

By means of DFT methods, we investigated the complexes formed between the fully deprotonated and the N-monoprotonated forms of EDTA (see section S1.1 and Fig. S15 for details). According to the experimental pKa values of EDTA, the fully deprotonated form predominates at pH > 10, while the *N*-monoprotonated form is dominant at pH  $\approx$  8. Theoretical calculations confirm the EDTA capability for complexing the Ag<sup>+</sup> cations in solution. The binding interaction is stronger (more stabilizing) for the fully deprotonated form at pH > 10 compared to the N-protonated form at pH = 8 ( $\Delta E_{binding} = -16.6$  kcal/mol vs -12.5 kcal/mol, see Section S1.2 and Fig. S16). This enhanced stability is attributed to the higher anionic character of the deprotonated form, which increases the stabilization of the cation charge. Both complexes show similar geometrical arrangements (Fig. 7), where EDTA hexacoordinate the central Ag<sup>+</sup> cation through interactions with four oxygen atoms of the carboxylic groups and the two nitrogen atoms. However, one of these nitrogen interactions is lost in the N-protonate complex.

– *Influence of the solution pH on the growth kinetics*. As shown in Fig. 2, precise control of the solution pH within the range of 8.1 and 10.5, while keeping other parameters constant, enables precise tailoring of the optical properties over a wide wavelength range. Slower growth kinetics favor the preferential addition of atoms within entrance grooves formed at stacking fault regions. Consequently, crystal growth predominantly occurs along the [111] direction and parallel to the {1 1 1} plane, as extensively reported in the literature [10,19,26–28].

- Crystalline structure of the seed and its evolution into AgNPTs with stacking faults. Our research suggests that inherent stacking defects in the seeds may not be essential. It has been proposed that a delicate interplay between kinetics and selective surface passivation may promote the emergence of twin planes, similar to those observed in Au decahedra and triangles, during the growth over single-crystalline gold nanoparticles of quasi-spherical shape [43]. In the present case, considering the essential role of EDTA in promoting the nanoplate morphology, we propose that the complexation of silver ions with EDTA, along with the different

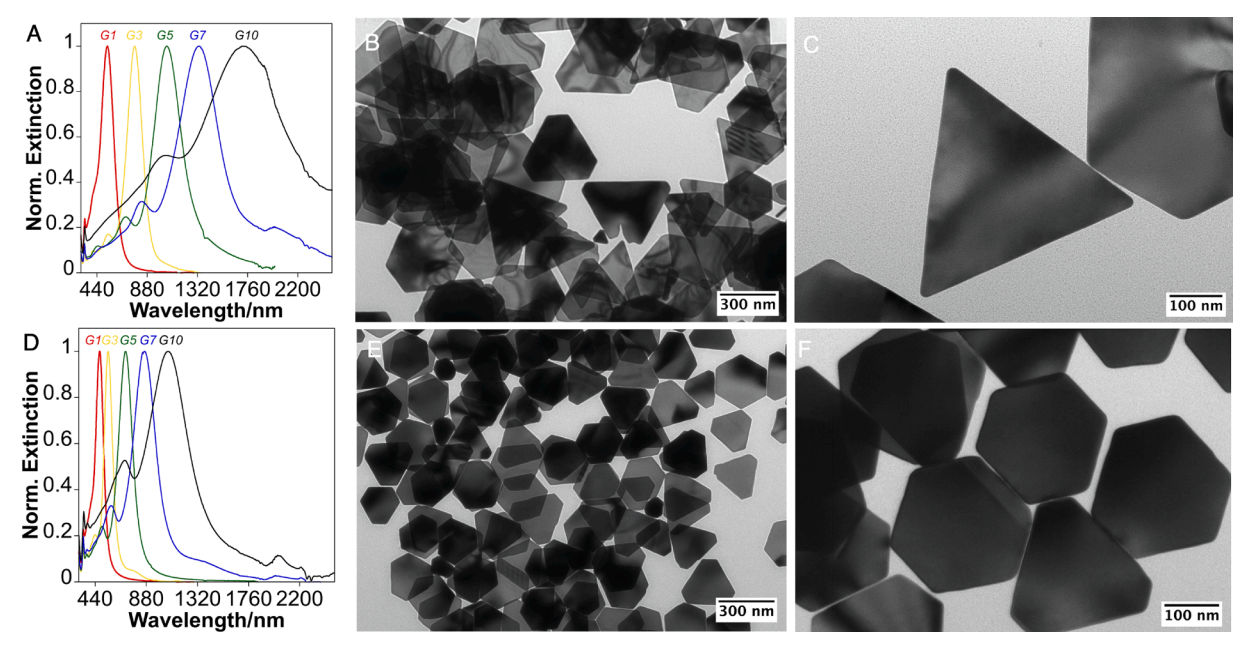
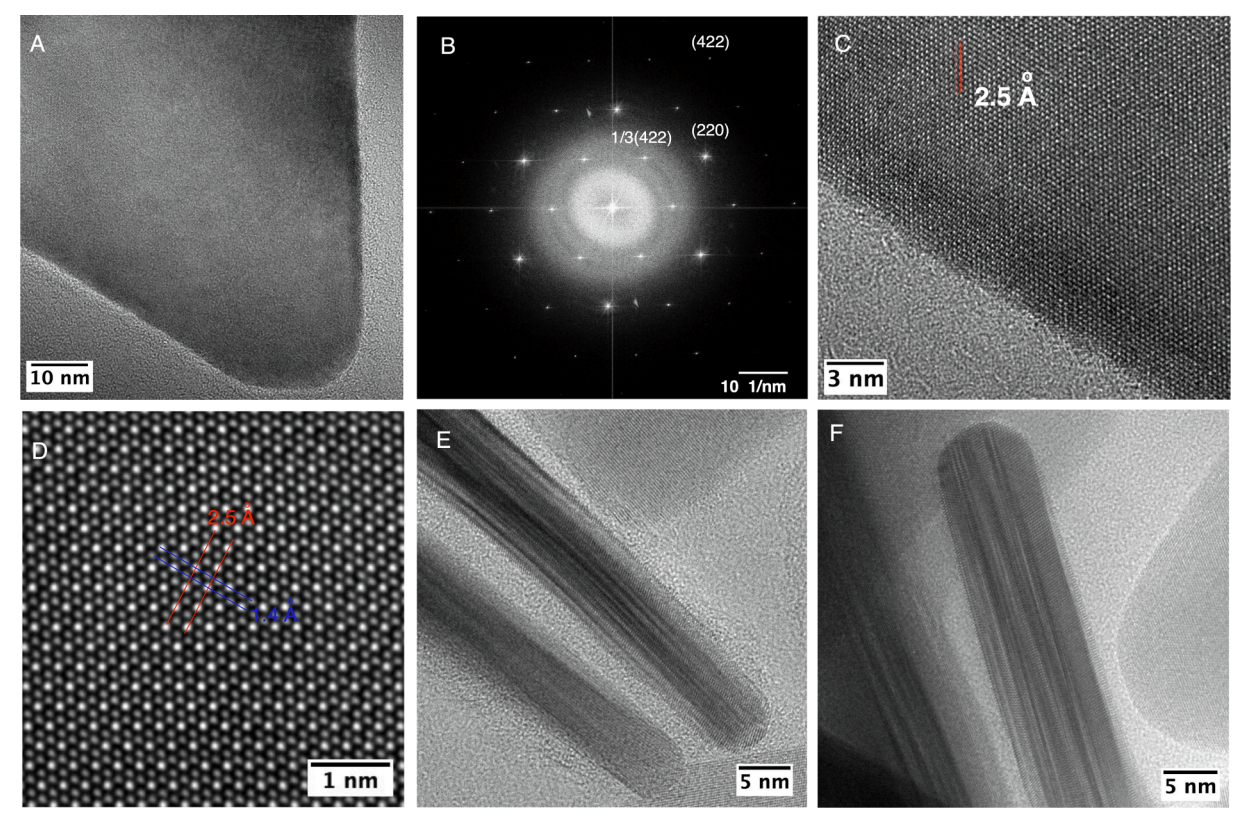


Fig. 5. UV-Vis-NIR spectra of nanoplates obtained during multigrowth (G1 to G10) and TEM images of the final growth produced using [AMP] of 0.15 mM (A-C) and 0.6 mM (D-F).



**Fig. 6.** (A) Bright-field HRTEM image of one AgNPT resting horizontally on the substrate with its triangular faces aligned perpendicular to the electron beam. (B) Fast Fourier Transform (FFT) of image A, where the bright spots are allowed {2 2 0} Bragg reflections and the six sharp weak spots are indexed as 1/3{4 2 2}. (C, D) Atomic resolution TEM images showing interplanar distances of 2.5 Å and 1.4 Å corresponding to 1/3{4 2 2} forbidden reflections and {2 2 0} Bragg reflections, respectively. (E, F) HRTEM image of a stack of vertically oriented AgNPTs, showing defect structure.

adsorption affinities of EDTA towards various crystalline facets of silver, facilitates the formation of twin planes and the plate-like structures.

Theoretical density functional tight binding computations were employed to analyze the energetic stabilization resulting from the EDTA adsorption on various silver surfaces. To this purpose, we studied the

adsorption of the deprotonated and N-monoprotonated EDTA forms on slabs mimicking the {1 1 1}, {1 1 0} and {1 0 0} silver surfaces (see Section S1.3 and Fig. S17 in SI). Our results indicated that at pH > 10, the adsorption of fully deprotonated EDTA is energetically favored over the adsorption of the N-monoprotonated species at lower pH on all

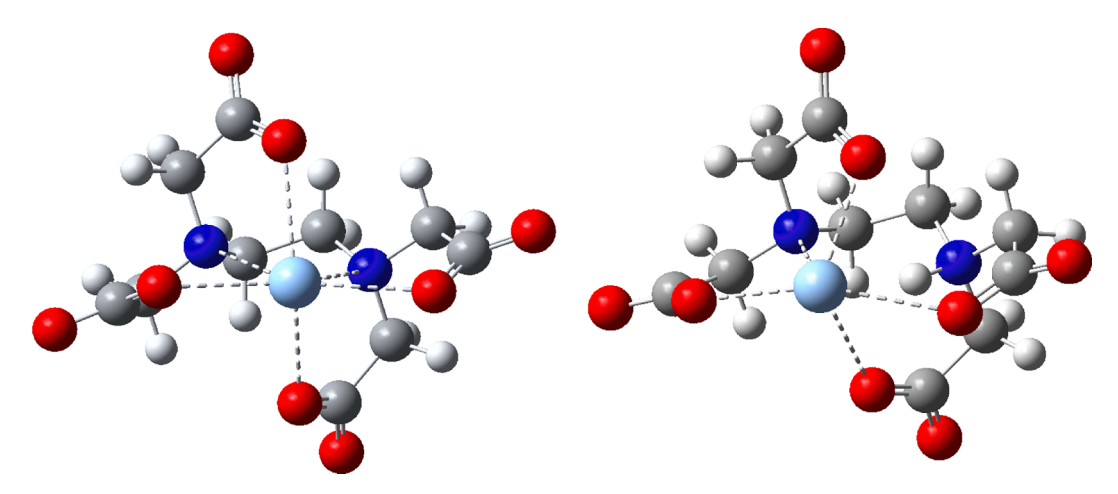


Fig. 7.  $M062X/6-311+G^{**}$  optimized geometries for Ag···EDTA complexes at pH > 10 (left) and pH  $\approx 8$  (right).

facets. To further analyze the effect of these interactions on the relative stability of each facet we have also computed adsorbed modified-surface energies,  $\gamma_{ads}$ , (see SI for details). Table 1 shows that the surface energy ordering for clean surfaces is maintained for systems with adsorbed EDTA, that is,  $\gamma\{1\ 1\ 1\} < \gamma\{1\ 0\ 0\} < \gamma\{1\ 1\ 0\}$ . However, EDTA adsorption significantly enhances the relative stabilization of the {1 1 1} surface compared to the  $\{1\ 0\ 0\}$  and  $\{1\ 1\ 0\}$  facets between  $7\ \%$  (pH = 8) and 20 % (pH > 10). This increased stability of the  $\{1\ 1\ 1\}$  facets due to EDTA adsorption promotes their greater exposure in the final shape of the nanoparticle, as observed for triangular and hexagonal nanoplates. Interestingly, a similar theoretical study for AMP adsorbed on silver surfaces (see Section S1.3 and Fig. S18 in SI) indicates lower adsorption energies compared to EDTA adsorption, suggesting that EDTA may exert a more pronounced influence on the final nanoparticle shape. Furthermore, the modified adsorbed surface energies (Table 1) suggest that the AMP adsorption reduce the preference for the {1 1 1} facet compared to EDTA, implying that nanoparticles with lesser {1 1 1} surface exposure would be expected.

– Vertical versus lateral growth: preferential adsorption of AMP. Precise control of nanoplate thickness can be achieved through the combined use of EDTA and AMP. Experimental findings indicate that AMP promotes vertical growth while maintaining the growth kinetics primarily influenced by pH. This effect is attributed to the preferential adsorption of AMP on  $\{1\ 0\ 0\}$  or  $\{1\ 1\ 0\}$  crystal facets, contrasting with  $\{1\ 1\ 1\}$  facets where EDTA adsorption significantly stabilizes these surfaces. Consequently, nanoparticles with adsorbed AMP exhibit a greater proportion of  $\{1\ 0\ 0\}$  and  $\{1\ 1\ 0\}$  facets than those with EDTA alone, resulting in thicker nanoplates at higher [AMP].

To analyze the different evolution of the nanoparticle shape influenced by adsorbed EDTA and AMP, we employed equilibrium Wulff constructions based on theoretical adsorbed modified surface energies. This approach defined theoretical triangular and hexagonal Wulff shapes constrained by top/bottom  $\{1\ 1\ 1\}$  facets and lateral  $\{1\ 1\ 0\}$  and  $\{1\ 0\ 0\}$  facets (see Section S1.4 and Fig. S19 in SI for further details). The effect of adsorption on  $\{1\ 1\ 1\}$  facets on the nanoparticle growth was modeled by over-stabilizing the  $\{1\ 1\ 1\}$  facets through the increase of

Table 1 Theoretical relative surface energies for low-index facets of clean silver surfaces ( $\gamma$ ) and with adsorbed EDTA and AMP ( $\gamma_{ads}$ ).

|                 | γ<br>Clean Ag | γ <sub>ads</sub><br>EDTA…Ag |         | γ <sub>ads</sub><br>AMP…Ag |
|-----------------|---------------|-----------------------------|---------|----------------------------|
|                 |               | pH = 8                      | pH > 10 |                            |
| {1 0 0}/{1 1 1} | 1.07          | 1.11                        | 1.24    | 1.03                       |
| {1 1 0}/{1 1 1} | 1.13          | 1.19                        | 1.32    | 1.00                       |
| {1 1 1}         | 1.00          | 1.00                        | 1.00    | 1.00                       |

the 1 1 1/1 1 0 surface energy ratio. Fig. 8 illustrates how theoretical Wulff constructions, derived from EDTA and AMP adsorbed-modified surface energies, evolve from initial truncated shapes limited by small top/bottom triangles to shapes resembling the experimental ones, dominated by large triangular top/bottom {1 1 1} facets and with smaller lateral {1 0 0} facets. Interestingly, Fig. 8 reveals that while the evolution of Wulff constructions based on EDTA and AMP-adsorbed surface energies follows similar structural patterns, the amount of {1 1 1} surfaces limiting the nanoparticle shape is clearly larger for EDTA than for AMP. Consequently, the lateral surface of the nanoparticle determined by the {1 1 0} and {1 0 0} facets is larger in AMP-adsorbed systems, consistent not only with the thicker nanoplates but also with a higher degree of truncation obtained in the presence of increasing [AMP].

# 3. Conclusions

We have developed an innovative seed-mediated synthesis method that produces high-performance truncated AgNPTs. Starting with singlecrystal silver seeds approximately 4-5 nm in size, we induce overgrowth using AA and EDTA, achieving nanoplates with distinct optical responses and well-defined morphologies. By adjusting the growth conditions, we can precisely control the size and thickness of the nanoplates, manipulating their aspect ratios and localized surface plasmon resonance (LSPR) properties. The use of AMP further allows for fine-tuning of the thickness and optical response of the nanoplates. Our findings reveal that the controlled growth of Ag seeds leads to the formation of nanoparticles with nanoplate morphology, challenging previous assumptions about the role of stacking defects. This work not only elucidates the formation mechanism of AgNPTs but also enables the production of customized plasmonic nanomaterials with adjustable morphologies and optical properties, establishing a foundation for advancements in the field of nanoplasmonics.

# 4. Materials and methods

# 4.1. Materials

Silver nitrate (AgNO<sub>3</sub>, 99 %, CAS: 7761-88-8) and deuterium oxide (D<sub>2</sub>O, 99 %) were obtained from Alfa Aesar. Ethylenediaminetetraacetic acid tetrasodium salt hydrate (EDTA, 99 %, CAS: 194491-31-1), Adenosine 5'-monophosphate disodium salt (AMP,  $\geq$ 99 %, CAS: 4578-31-8), phosphoric acid (H<sub>3</sub>PO<sub>4</sub>,  $\geq$ 99 %, CAS: 7664-38-2), sodium hydroxide (NaOH,  $\geq$ 98 %, CAS: 1310-73-2) and sodium borohydride (NaBH<sub>4</sub>,  $\geq$ 99 %, reagent plus, CAS: 16940-66-2) were supplied by Merck.  $\mbox{\tiny $L$}$ -Ascorbic acid ( $\geq$ 99 %, CAS: 50-81-7) was obtained from Thermo Fisher Scientific. Ultra-pure water (Type I, produced using a Millipore Simplicity UV

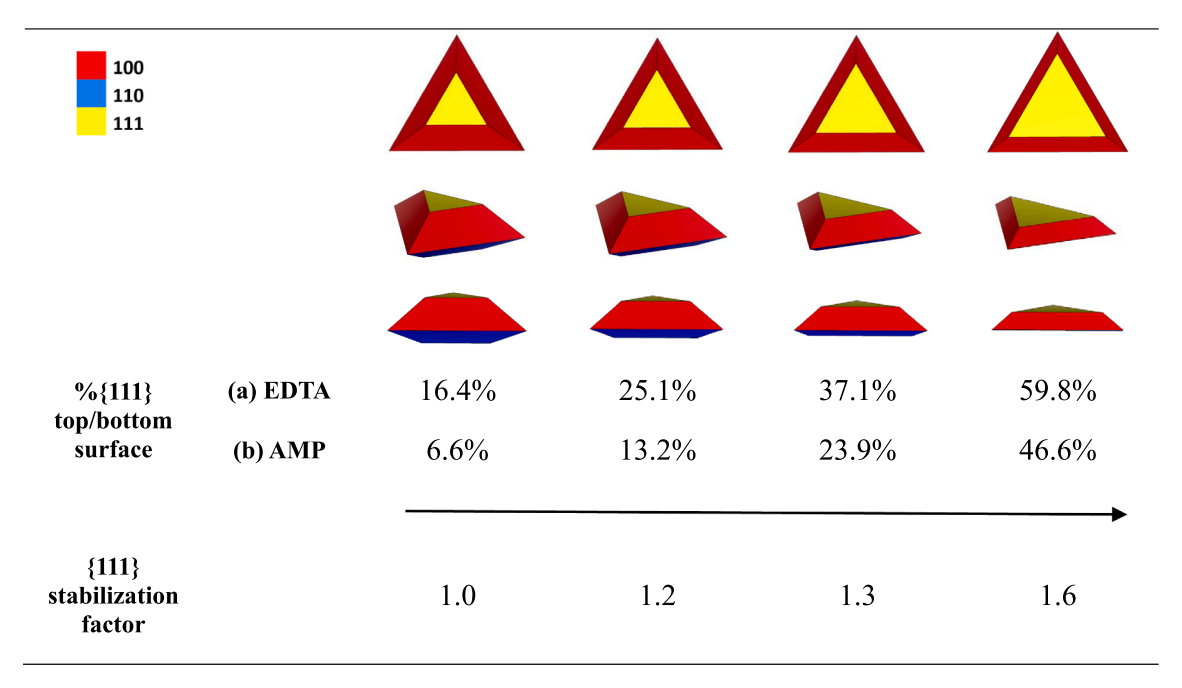


Fig. 8. Theoretical Wulff constructions showing the evolution of a triangular nanoplate when the  $\{1\ 1\ 1\}$  surface is over-stabilized. The over-stabilization of the  $\{1\ 1\ 1\}$  surface is determined by a factor that multiplies the ratio between the adsorbed-modified surface energies  $\{1\ 1\ 1\}/\{1\ 0\ 0\}$ . The table includes the amount of triangular  $\{1\ 1\ 1\}$  top/bottom surfaces limiting the Wulff shape computed from (a) EDTA and (b) AMP adsorbed modified surface energies.

system) was used in all preparations.

#### 4.2. Characterization

UV-visible-NIR extinction spectra were recorded using an Agilent 8453 or JASCO 770 spectrophotometer with quartz cells of 0.2, 0.25, or 0.5 cm optical path length. To obtain spectra of nanoplates over 1350 nm, the samples were centrifuged twice using D2O as solvent (Nanoplates produced solely with EDTA were functionalized with PEG-SH before the purification in D2O. Nanoplates obtained in the presence of AMP were purified using a deuterium oxide solution of NaOH 2 mM). The extinction spectra were measured using a quartz cell with a  $0.1\ cm$ optical path length. Low-resolution TEM images were obtained with a JEOL JEM 1010 transmission electron microscope operating at an acceleration voltage of 100 kV, utilizing copper or gold grids with thin carbon film to deposit the samples (CACTI-UVigo User Facilities). The average size of lateral dimension of the nanoplates was analyzed using low-resolution TEM images counting between 100-200 nanoplates per sample (Fig. S20 shows the method for measuring the size of nanoplates). HRTEM of silver seeds was carried out using a FEI Titan ChemiSTEM transmission electron microscope operated at 200 kV (INL User Facilities), using gold grids coated with a thin carbon film to deposit the silver seeds. For HRTEM images of nanoplates characterization, a TEM-TITAN 60-300 kV from Thermo Fisher Scientific equipped with an aberration corrector was used (NanoGune User Facilities). A New Era Pump System, Model 100, was used to carry out the synthesis of the seeds. The pH of the reactions was measured using a pH meter (HACH-SensION pH31), obtaining the pH values at the end of the nanoplate growth in all cases.

# 4.3. Synthesis of silver seeds

The synthesis was conducted at a controlled room temperature of 21  $^{\circ}\text{C}.$  A 25 mL opaque vial containing a small oval stirrer bar (15x7 mm) was filled with 14.7 mL of water. Subsequently, 300  $\mu\text{L}$  of a freshly prepared 20 mM NaBH4 solution was added. Without delay and under vigorous magnetic stirring (~1200 rpm), 5 mL of a freshly prepared aqueous solution, composed of 4.7 mL of water, 0.2 mL of 20 mM EDTA,

and 0.1 mL of 20 mM AgNO<sub>3</sub>, was introduced dropwise using an infusion pump at a rate of 1 mL/min. The vial was then covered with a cap (not fully screwed on), and the stirring was maintained for 2 h (Fig. S21 shows the set-up employed). Finally, the stirrer bar was removed, and the vial was stored at  $\sim\!\!5$  °C covered to protect it from light for 8 h to facilitate the decomposition of excess NaBH<sub>4</sub>. The seeds solution was used without any purification steps and showed comparable results for at least one week when stored at  $\sim\!\!5$  °C.

# 4.4. Synthesis of truncated silver nanoplates

The nanoplates were synthesized in a 25 mL round-bottom reaction flask under magnetic stirring and normal light laboratory conditions at room temperature (21 °C). The stock solutions were used at a concentration of 20 mM, and the total reaction volume was maintained at 20 mL in all cases. Briefly,  $0.15\,mL$  of AgNO $_3$  and  $0.6\,mL$  EDTA were added to 18.95 mL of water. After 1 min stirring, 0.15 mL of AA and immediately 0.15 mL of silver seed were injected. The reaction was moderately stirred for 1 h a RT (see Scheme S1). To obtain changes in the pH, different volumes of H<sub>3</sub>PO<sub>4</sub> (between 5 and 150 µL to produce a final pH between 7 and 9.2) or NaOH (between 50 and 600  $\mu L$  to produce more basic pHs) were injected before the addition of AA. A growth medium with pH over 12 was produced using a stock solution of NaOH of  $0.2\,\mathrm{M}$ . The pH of the reactions was measured at the end of the nanoplate growth in all cases. For the nanoplates produced in the presence of AMP, different volumes of a freshly prepared AMP aqueous solution (between 0.075 and 0.7 mL) were used, which were subsequently added to the EDTA. In these cases, the reactions were moderately stirred for 2 h a RT (see Scheme S1). At the end of growth, an additional amount of 0.3 mL of AMP 20 mM was added keeping the solution under stirring for 1 h before purification. The nanoplates were then purified by repeated centrifugations (between 3500 rpm and 8500 rpm, depending on their size) using NaOH aqueous solution (2 mM) as solvent. Samples were finally stored in 1 mM NaOH at  $\sim$ 5°C and covered from light.

# 4.5. Overgrowth of silver nanoplates

The overgrowth of the nanoplates was carried out in a round-bottom

reaction flask under magnetic stirring and was performed in a total volume of 20 mL in all cases. [AgNO $_3$ ] (0.15 mM), [EDTA] (0.6 mM) and AA (0.15 mM) were maintained constant in all growth mediums without considering the amount transferred in the volume of nanoplate used as seed. Different volumes of seeds or nanoplate were used as referred to in the main text.

#### 4.6. Overgrowth in presence of AMP

We conducted two series of multi-growth experiments using two different concentrations of AMP to generate nanoplates of varying size and thickness. Throughout all growth mediums, the concentrations of [AgNO<sub>3</sub>] (0.15 mM), [EDTA] (0.6 mM), AA (0.15 mM) and AMP (0.15 or 0.6 mM) were kept constant, regardless of the quantity of these reagents transferred into the volume of nanoplate used as a seed in subsequent growth stages. However, the concentration of  $\rm H_3PO_4$  was maintained at 0.085 mM in all cases, considering the amount of  $\rm H_3PO_4$  transferred into the volume of nanoplate used as a seed in subsequent growth stages (see Scheme S2). At the end of each growth, an additional amount of 0.3 mL of AMP 20 mM was added keeping the solution under stirring for 1 h before purification. The nanoplates were then purified by repeated centrifugations cycles (between 1500 and 8500 rpm, depending on their size) using NaOH aqueous solution (2 mM) as solvent.

## 4.7. Computational methods

The stable conformers of the different protonated forms of EDTA and its complexes with the silver cation have been obtained employing the M062X functional with the  $6\text{-}311\text{+}G^{**}$  basis set and the SMD implicit solvation method (see Section S1.1 and Fig. S16 in S1 for details). Since implicit models do not consider the specific interactions between solutes and water, a cavity scaling parameter of 0.90 was used for anionic species to obtain more accurate results. All the optimized geometries obtained were characterized as energy minima by computation of their harmonic vibrational frequencies using Gaussian16 [44].

The interaction between EDTA and AMP and the metallic nanoparticle has been studied using the GFN1 xTB density functional tight binding method [45] with periodic boundary conditions as implemented in the DFTB+ program [46]. The three lower-index facets {1 1 1}, {1 1 0}, {1 0 0} has been modelled by using the slabs described in Table S4 together with a vacuum layer over the top surface of 35 Å to avoid molecular lateral interactions. The adsorption of EDTA and AMP has been studied by performing geometrical optimizations of the adsorbates while maintaining fixed the metal structure. Geometrical optimizations of many different initial configurations have been performed at the  $\Gamma$ -point and final energies were obtained using a Brillouin  $15\times15\times1$  grid. Adsorption energies for the most stable configurations found were obtained by computing the energy difference

$$E_{\text{ads}} = E_{(\text{adsorbate} \cdots \text{slab})} - E_{(\text{adsorbate})} - E_{\{\text{slab}\}}$$

Surface energies,  $\gamma$ , were obtained using the GFN1-xTB method with a Brillouin  $15 \times 15 \times 1$  grid employing the experimental silver geometry and increasing the number of silver layers until energy convergence. Adsorbed-modified surface energies,  $\gamma_{ads}$ , for those systems containing EDTA and AMP have been obtained according to

$$\gamma_{ads} = \gamma + \frac{E_{ads}}{2A}$$

where  $\gamma$  are the surface energies for clean surfaces,  $E_{ads}$  is the adsorption energy of EDTA on a given silver facet and A is the surface of the slab chosen to mimic the silver surface. Relative surface energies were obtained with respect to the most stable {111} facet through {110}/{111} and {100}/{111} relations.

#### **Author Contributions**

The manuscript was written through contributions of all authors. All authors have given approval to the final version of the manuscript.

## **Funding Sources**

The authors thank the financial support from national funds (FCT/ MCTES, Fundação para a Ciência e Tecnologia and Ministério da Ciência, Tecnologia e Ensino Superior) through project SiSi4Bacter (PTDC/ QUI-COL/1517/2020), and the financial support by the Associate Laboratory Research Unit for Green Chemistry-Clean Processes and Technologies-LAQV which is financed by national funds from FCT/MEC (UID/QUI/50006/2013) and co-financed by the ERDF under the PT2020 Partnership Agreement (POCI-01-0145-FEDER-007265), FCT/ MCTES (LA/P/0008/2020 DOI 10.54499/LA/P/0008/2020, UIDP/ 50006/2020 DOI 10.54499/UIDP/50006/2020 and UIDB/50006/2020 DOI 10.54499/UIDB/50006/2020), through national funds, as well as the PROTEOMASS Scientific Society General Funds (Portugal) for funding (Grant 2023-2024) support. J.P.J. and I.P.S. acknowledge the support from the FET Open grant agreement no.965018 (BIOCELLPHE). MICIU/AEI /10.13039/501100011033 and FEDER/EU (Grant No: PID2022-138724NB-I00). I. P.J. acknowledges the support from MICIU/ AEI /10.13039/501100011033 and FEDER/EU (Grant No: PID2022-138023NB-I00). A.F.L. thanks the FCT/MCTES (Fundação para a Ciência e Tecnologia and Ministério da Ciência, Tecnologia e Ensino Superior) for the research contract through the project PTDC/QUI-COL/ 1517/2020. S.N. thanks the FCT/MCTEC (Fundação para a Ciência e Tecnologia and Ministério da Ciência, Tecnologia e Ensino Superior) Portugal for her doctoral grant associated with the Chemistry PhD program (SFRH/BD/144618/2019).

# CRediT authorship contribution statement

Adrián Fernández-Lodeiro: Writing - review & editing, Writing original draft, Visualization, Validation, Supervision, Resources, Methodology, Investigation, Funding acquisition, Data curation, Conceptualization. Carlos Fernández-Lodeiro: Writing - review & editing, Writing - original draft, Visualization, Validation, Supervision, Resources, Methodology, Investigation, Funding acquisition, Data curation, Conceptualization. Silvia Nuti: Writing - review & editing, Validation, Methodology, Investigation, Data curation. Ignacio Pérez-Juste: Writing – review & editing, Visualization, Resources, Investigation, Formal analysis. Isabel Pastoriza-Santos: Writing - review & editing, Resources, Investigation, Funding acquisition, Formal analysis. Jorge Pérez-Juste: Writing - review & editing, Writing - original draft, Supervision, Resources, Funding acquisition, Formal analysis, Conceptualization. Enrique Carbo-Argibay: Writing - review & editing, Visualization, Investigation, Data curation. José L. Capelo: Writing review & editing, Resources. Carlos Lodeiro: Writing - review & editing, Resources, Funding acquisition, Data curation. Javier Fernández-Lodeiro: Writing - review & editing, Writing - original draft, Visualization, Validation, Supervision, Resources, Methodology, Investigation, Funding acquisition, Data curation, Conceptualization.

# Declaration of competing interest

The authors declare that they have no known competing financial interests or personal relationships that could have appeared to influence the work reported in this paper.

# Acknowledgments

J.F.-L. thanks the FCT-UNL for the research contract through the Program DL57/2016 Norma Transitória. This work was carried out in part through the use of the INL User Facilities. The authors thank Dr.

Jamila Djafari for her assistance with the design of the TOC.

## Appendix A. Supplementary data

The supplementary information includes a bibliographic table of key nanoplate synthesis methods, comprehensive characterizations such as High-Resolution Transmission Electron Microscopy (HRTEM) and Transmission Electron Microscopy (TEM) images, and extinction spectra of nanoplates synthesized under various conditions, including increased seed amounts, different pH levels, various concentrations of AMP, and multigrowth of nanoplates. It also contains detailed time-resolved spectroscopic kinetic studies conducted in the presence of AMP, Atomic Force Microscopy (AFM) images of nanoplates obtained after multigrowth experiments, and theoretical Wulff reconstructions illustrating the morphology evolution of hexagonal nanoplates. Supplementary data to this article can be found online at https://doi.org/10.10 16/j.jcis.2024.10.179.

# Data availability

Data will be made available on request.

#### References

- L. Scarabelli, M. Sun, X. Zhuo, S. Yoo, J.E. Millstone, M.R. Jones, L.M. Liz-Marzán, Plate-like colloidal metal nanoparticles, Chem. Rev. 123 (2023) 3493–3542, https://doi.org/10.1021/acs.chemrev.3c00033.
- [2] I. Pastoriza-Santos, L.M. Liz-Marzán, Colloidal silver nanoplates. State of the art and future challenges, J. Mater. Chem. 18 (2008) 1724, https://doi.org/10.1039/ b716538b
- [3] J.E. Millstone, S.J. Hurst, G.S. Métraux, J.I. Cutler, C.A. Mirkin, Colloidal gold and silver triangular nanoprisms, Small 5 (2009) 646–664, https://doi.org/10.1002/ smll 200801480
- [4] R. Jin, Y. Cao, C.A. Mirkin, K.L. Kelly, G.C. Schatz, J.G. Zheng, Photoinduced conversion of silver nanospheres to nanoprisms, Science 294 (2001) (1979) 1901–1903, https://doi.org/10.1126/science.1066541.
- [5] R. Jin, Y. Charles Cao, E. Hao, G.S. Métraux, G.C. Schatz, C.A. Mirkin, Controlling anisotropic nanoparticle growth through plasmon excitation, Nature 425 (2003) 487–490, https://doi.org/10.1038/nature02020.
- [6] B. Xue, D. Wang, J. Zuo, X. Kong, Y. Zhang, X. Liu, L. Tu, Y. Chang, C. Li, F. Wu, Q. Zeng, H. Zhao, H. Zhao, H. Zhang, Towards high quality triangular silver nanoprisms: improved synthesis, six-tip based hot spots and ultra-high local surface plasmon resonance sensitivity, Nanoscale 7 (2015) 8048–8057, https://doi.org/10.1039/C4NR06901C.
- [7] G.S. Métraux, C.A. Mirkin, Rapid thermal synthesis of silver nanoprisms with chemically tailorable thickness, Adv. Mater. 17 (2005) 412–415, https://doi.org/ 10.1002/adma.200401086.
- [8] Q. Zhang, Y. Yang, J. Li, R. Iurilli, S. Xie, D. Qin, Citrate-free synthesis of silver nanoplates and the mechanistic study, ACS Appl. Mater. Interfaces 5 (2013) 6333–6345, https://doi.org/10.1021/am401374x.
- [9] Y. Xiong, I. Washio, J. Chen, H. Cai, Z.-Y. Li, Y. Xia, Poly(vinyl pyrrolidone): a dual functional reductant and stabilizer for the facile synthesis of noble metal nanoplates in aqueous solutions, Langmuir 22 (2006) 8563–8570, https://doi.org/ 10.1021/la061323x.
- [10] Q. Zhang, Y. Hu, S. Guo, J. Goebl, Y. Yin, Seeded growth of uniform Ag nanoplates with high aspect ratio and widely tunable surface plasmon bands, Nano Lett. 10 (2010) 5037–5042, https://doi.org/10.1021/nl1032233.
- [11] I. Pastoriza-Santos, L.M. Liz-Marzán, Synthesis of silver nanoprisms in DMF, Nano Lett. 2 (2002) 903–905, https://doi.org/10.1021/nl025638i.
- [12] S. Chen, D.L. Carroll, Synthesis and characterization of truncated triangular silver nanoplates, Nano Lett. 2 (2002) 1003–1007, https://doi.org/10.1021/nl025674h.
- [13] C.-L. Lee, C.-M. Syu, H.-P. Chiou, C.-H. Chen, H.-L. Yang, High-yield, size-controlled synthesis of silver nanoplates and their applications as methanol-tolerant electrocatalysts in oxygen reduction reaction, Int. J. Hydrogen Energy 36 (2011) 10502–10512, https://doi.org/10.1016/j.ijhydene.2011.06.028.
- [14] C.-H. Zhang, J. Zhu, J.-J. Li, J.-W. Zhao, Small and sharp triangular silver nanoplates synthesized utilizing tiny triangular nuclei and their excellent SERS activity for selective detection of thiram residue in soil, ACS Appl. Mater. Interfaces 9 (2017) 17387–17398, https://doi.org/10.1021/acsami.7b04365.
- [15] Z. Yi, X. Li, X. Xu, B. Luo, J. Luo, W. Wu, Y. Yi, Y. Tang, Green, effective chemical route for the synthesis of silver nanoplates in tannic acid aqueous solution, Colloids Surf., A Physicochem. Eng. Asp. 392 (2011) 131–136, https://doi.org/10.1016/j. colsurfa.2011.09.045.
- [16] J. Yang, L. Lu, H. Wang, W. Shi, H. Zhang, Glycyl glycine templating synthesis of single-crystal silver nanoplates, Cryst. Growth Des. 6 (2006) 2155–2158, https:// doi.org/10.1021/cg060143i.
- [17] D. Aherne, D.M. Ledwith, M. Gara, J.M. Kelly, Optical properties and growth aspects of silver nanoprisms produced by a highly reproducible and rapid synthesis

- at room temperature, Adv. Funct. Mater. 18 (2008) 2005–2016, https://doi.org/
- [18] D.E. Charles, M. Gara, D. Aherne, D.M. Ledwith, J.M. Kelly, W.J. Blau, M. E. Brennan-Fournet, Scaling of surface plasmon resonances in triangular silver nanoplate sols for enhanced refractive index sensing, Plasmonics 6 (2011) 351–362, https://doi.org/10.1007/s11468-011-9211-x.
- [19] Z. Cao, H. Fu, L. Kang, L. Huang, T. Zhai, Y. Ma, J. Yao, Rapid room-temperature synthesis of silver nanoplates with tunable in-plane surface plasmon resonance from visible to near-IR, J. Mater. Chem. 18 (2008) 2673, https://doi.org/10.1039/ b800691a
- [20] B.-H. Kim, J.-H. Oh, S.H. Han, Y.-J. Yun, J.-S. Lee, Combinatorial polymer library approach for the synthesis of silver nanoplates, Chem. Mater. 24 (2012) 4424–4433, https://doi.org/10.1021/cm3028115.
- [21] T. Tan, C. Tian, Z. Ren, J. Yang, Y. Chen, L. Sun, Z. Li, A. Wu, J. Yin, H. Fu, LSPR-dependent SERS performance of silver nanoplates with highly stable and broad tunable LSPRs prepared through an improved seed-mediated strategy, Phys. Chem. Chem. Phys. 15 (2013) 21034, https://doi.org/10.1039/c3cp52236a.
- [22] J. Xie, J.Y. Lee, D.I.C. Wang, Y.P. Ting, Silver nanoplates: from biological to biomimetic synthesis, ACS Nano 1 (2007) 429–439, https://doi.org/10.1021/ pn7000883
- [23] V. Germain, J. Li, D. Ingert, Z.L. Wang, M.P. Pileni, Stacking faults in formation of silver nanodisks, J. Phys. Chem. B 107 (2003) 8717–8720, https://doi.org/ 10.1021/jp0303826.
- [24] T. Tan, S. Zhang, J. Wang, Y. Zheng, H. Lai, J. Liu, F. Qin, C. Wang, Resolving the stacking fault structure of silver nanoplates, Nanoscale 13 (2021) 195–205, https://doi.org/10.1039/D0NR06912D.
- [25] S.E. Skrabalak, Y. Xia, Pushing nanocrystal synthesis toward nanomanufacturing, ACS Nano 3 (2009) 10–15, https://doi.org/10.1021/nn800875p.
- [26] J. Zeng, J. Tao, W. Li, J. Grant, P. Wang, Y. Zhu, Y. Xia, A mechanistic study on the formation of silver nanoplates in the presence of silver seeds and citric acid or citrate ions, Chem. Asian J. 6 (2011) 376–379, https://doi.org/10.1002/ asia.201000728.
- [27] Y. Xiong, A.R. Siekkinen, J. Wang, Y. Yin, M.J. Kim, Y. Xia, Synthesis of silver nanoplates at high yields by slowing down the polyol reduction of silver nitrate with polyacrylamide, J. Mater. Chem. 17 (2007) 2600, https://doi.org/10.1039/ b705253g.
- [28] M.A. Mahmoud, Simultaneous reduction of metal ions by multiple reducing agents initiates the asymmetric growth of metallic nanocrystals, Cryst. Growth Des. 15 (2015) 4279–4286, https://doi.org/10.1021/acs.cgd.5b00592.
- [29] Y.N. Wijaya, J. Kim, W.M. Choi, S.H. Park, M.H. Kim, A systematic study of triangular silver nanoplates: one-pot green synthesis, chemical stability, and sensing application, Nanoscale 9 (2017) 11705–11712, https://doi.org/10.1039/ C7NR03077K.
- [30] X. Liu, L. Li, Y. Yang, Y. Yin, C. Gao, One-step growth of triangular silver nanoplates with predictable sizes on a large scale, Nanoscale 6 (2014) 4513, https://doi.org/10.1039/c4nr00254g.
- [31] D.E. Charles, D. Aherne, M. Gara, D.M. Ledwith, Y.K. Gun'ko, J.M. Kelly, W.J. Blau, M.E. Brennan-Fournet, Versatile solution phase triangular silver nanoplates for highly sensitive plasmon resonance sensing, ACS Nano 4 (2010) 55–64. 10.1021/ nn9016235.
- [32] Z. Yi, J. Zhang, H. He, X. Xu, B. Luo, X. Li, K. Li, G. Niu, X. Tan, J. Luo, Y. Tang, W. Wu, Y. Yi, Convenient synthesis of silver nanoplates with adjustable size through seed mediated growth approach, Trans. Nonferrous Met. Soc. Chin. 22 (2012) 865–872, https://doi.org/10.1016/S1003-6326(11)61258-2.
- [33] N. Li, Q. Zhang, S. Quinlivan, J. Goebl, Y. Gan, Y. Yin, H<sub>2</sub>O<sub>2</sub>-aided seed-mediated synthesis of silver nanoplates with improved yield and efficiency, ChemPhysChem 13 (2012) 2526–2530, https://doi.org/10.1002/cphc.201101018.
- [34] J. Zeng, X. Xia, M. Rycenga, P. Henneghan, Q. Li, Y. Xia, Successive deposition of silver on silver nanoplates: lateral versus vertical growth, Angew. Chem. Int. Ed. 50 (2011) 244–249, https://doi.org/10.1002/anie.201005549.
- [35] M.H. Kim, J.-J. Lee, J.-B. Lee, K.-Y. Choi, Synthesis of silver nanoplates with controlled shapes by reducing silver nitrate with poly(vinyl pyrrolidone) in Nmethylpyrrolidone, CrstEngComm 15 (2013) 4660, https://doi.org/10.1039/ c2se40006d
- [36] Y. Liu, Q. Song, Z. Xu, Selective extraction of silver and palladium in leachate based on EDTA Complexation: electrodeposition, nucleation mechanism, and kinetic analysis, ACS Sustain. Chem. Eng. 10 (2022) 16647–16656, https://doi. org/10.1021/acssuschemeng.2c04479.
- [37] G.M. de Oliveira, L.L. Barbosa, R.L. Broggi, I.A. Carlos, Voltammetric study of the influence of EDTA on the silver electrodeposition and morphological and structural characterization of silver films, J. Electroanal. Chem. 578 (2005) 151–158, https:// doi.org/10.1016/j.jelechem.2004.12.033.
- [38] A. Sánchez-Iglesias, N. Winckelmans, T. Altantzis, S. Bals, M. Grzelczak, L.M. Liz-Marzán, High-yield seeded growth of monodisperse pentatwinned gold nanoparticles through thermally induced seed twinning, J. Am. Chem. Soc. 139 (2017) 107–110, https://doi.org/10.1021/jacs.6b12143.
- [39] C. Fernández-Lodeiro, R. Tambosi, J. Fernández-Lodeiro, A. Fernández-Lodeiro, S. Nuti, S. Ouchane, N. Kébaïli, J. Pérez-Juste, I. Pastoriza-Santos, C. Lodeiro, Adenosine-monophosphate-assisted homogeneous silica coating of silver nanoparticles in high yield, Nanomaterials 13 (2023) 2788, https://doi.org/ 10.3390/nanol3202788.
- [40] C. Fernández-Lodeiro, J. Fernández-Lodeiro, A. Fernández-Lodeiro, S. Nuti, C. Lodeiro, A. LaGrow, I. Pérez-Juste, J. Pérez-Juste, I. Pastoriza-Santos, Synthesis of tuneable gold nanostars: the role of adenosine monophosphate, J Mater Chem C Mater 11 (2023) 12626–12636, https://doi.org/10.1039/D3TC01567J.

- [41] M.T. Friend, N.A. Wall, Stability constants for Zirconium(IV) complexes with EDTA, CDTA, and DTPA in perchloric acid solutions, Inorg. Chim. Acta 484 (2019) 357–367, https://doi.org/10.1016/j.ica.2018.09.034.
- [42] L.C. O'Brien, H.B. Root, C.C. Wei, D. Jensen, N. Shabestary, C. De Meo, D.J. Eder, M<sup>2+</sup> EDTA binding affinities: a modern experiment in thermodynamics for the physical chemistry laboratory, J. Chem. Educ. 92 (2015) 1547–1551, https://doi.org/10.1021/acs.jchemed.5b00159.
- [43] M. Grzelczak, A. Sánchez-Iglesias, H. Heidari, S. Bals, I. Pastoriza-Santos, J. Pérez-Juste, L.M. Liz-Marzán, Silver ions direct twin-plane formation during the overgrowth of single-crystal gold nanoparticles, ACS Omega 1 (2016) 177–181, https://doi.org/10.1021/acsomega.6b00066.
- [44] Frisch, M. J.; Trucks, G. W.; Schlegel, H. B.; Scuseria, G. E.; Robb, M. A.; Cheeseman, J. R.; Scalmani, G.; Barone, V.; Petersson, G. A.; Nakatsuji, H.; Li, X.; Caricato, M.; Marenich, A. V.; Bloino, J.; Janesko, B. G.; Gomperts, R.; Mennucci, B.; Hratchian, H. P.; Ortiz, J. V.; Izmaylov, A. F.; Sonnenberg, J. L.; Williams-Young, D.; Ding, F.; Lipparini, F.; Egidi, F.; Goings, J.; Peng, B.; Petrone, A.; Henderson, T.; Ranasinghe, D.; Zakrzewski, V. G.; Gao, J.; Rega, N.; Zheng, G.; Liang, W.; Hada, M.; Ehara, M.; Toyota, K.; Fukuda, R.; Hasegawa, J.; Ishida, M.; Nakajima, T.; Honda, Y.; Kitao, O.; Nakai, H.; Vreven, T.; Throssell, K.;
- Montgomery, J. A., Jr.; Peralta, J. E.; Ogliaro, F.; Bearpark, M. J.; Heyd, J. J.; Brothers, E. N.; Kudin, K. N.; Staroverov, V. N.; Keith, T. A.; Kobayashi, R.; Normand, J.; Raghavachari, K.; Rendell, A. P.; Burant, J. C.; Iyengar, S. S.; Tomasi, J.; Cossi, M.; Millam, J. M.; Klene, M.; Adamo, C.; Cammi, R.; Ochterski, J. W.; Martin, R. L.; Morokuma, K.; Farkas, O.; Foresman, J. B.; Fox, D. J. Gaussian 16, Revision C.01, Gaussian, Inc., Wallingford CT, 2016.
- [45] C. Bannwarth, E. Caldeweyher, S. Ehlert, A. Hansen, P. Pracht, J. Seibert, S. Spicher, S. Grimme, Extended <scp>tight-binding</scp> quantum chemistry methods, WIREs Comput. Mol. Sci. 11 (2021), https://doi.org/10.1002/ wcms.1493.
- [46] B. Hourahine, B. Aradi, V. Blum, F. Bonafé, A. Buccheri, C. Camacho, C. Cevallos, M.Y. Deshaye, T. Dumitrică, A. Dominguez, S. Ehlert, M. Elstner, T. van der Heide, J. Hermann, S. Irle, J.J. Kranz, C. Köhler, T. Kowalczyk, T. Kubař, I.S. Lee, V. Lutsker, R.J. Maurer, S.K. Min, I. Mitchell, C. Negre, T.A. Niehaus, A.M. N. Niklasson, A.J. Page, A. Pecchia, G. Penazzi, M.P. Persson, J. Řezáč, C. G. Sánchez, M. Sternberg, M. Stöhr, F. Stuckenberg, A. Tkatchenko, V.W.Z. Yu, T. Frauenheim, DFTB+, a software package for efficient approximate density functional theory based atomistic simulations, J. Chem. Phys. 152 (2020), https://doi.org/10.1063/1.5143190.